Published for SISSA by Springer

Received: January 26, 2022
Revised: March 22, 2022
Accepted: April 11, 2022
Published: May 11, 2022

Search for the decay $B^0 \to \phi\mu^+\mu^-$

The LHCb collaboration

E-mail: yilong.wang@cern.ch

Abstract: A search for the decay $B^0 \to \phi\mu^+\mu^-$ is performed using proton-proton collisions at centre-of-mass energies of 7, 8, and 13 TeV collected by the LHCb experiment and corresponding to an integrated luminosity of $9\,\text{fb}^{-1}$. No evidence for the $B^0 \to \phi\mu^+\mu^-$ decay is found and an upper limit on the branching fraction, excluding the ϕ and charmonium regions in the dimuon spectrum, of 4.4×10^{-3} at a 90% credibility level, relative to that of the $B^0_s \to \phi\mu^+\mu^-$ decay, is established. Using the measured $B^0_s \to \phi\mu^+\mu^-$ branching fraction and assuming a phase-space model, the absolute branching fraction of the decay $B^0 \to \phi\mu^+\mu^-$ in the full q^2 range is determined to be less than 3.2×10^{-9} at a 90% credibility level.

Keywords: B Physics, Branching fraction, Hadron-Hadron Scattering , Rare Decay

ArXiv ePrint: 2201.10167

https://doi.org/10.1007/JHEP05(2022)067

JHEP05(2022)067

Contents

JHEP05(2022)067

1 Introduction

The decay $B^0 \to \phi\mu^+\mu^-$ proceeds mainly via the color-suppressed penguin annihilation diagrams (a), (b), and (c) in figure 1, if we consider only the $s\bar{s}$ component of the ϕ meson. Annihilation decays of B mesons are strongly suppressed in the Standard Model (SM) but very sensitive to physics beyond the SM. The annihilation contribution to the $B^0 \to \phi\mu^+\mu^-$ branching fraction is estimated to be approximately of the order of 10^{-12} in the QCD factorization approach [1]. However, when using this decay to probe new physics, the contribution from the small $d\bar{d}$ component of the ϕ meson must be considered. Contributions from $\omega - \phi$ mixing, figure 1 (d), and new physics could have significant effects on this decay. There is no theoretical study of these effects in the literature. Some clues can be found in the reported studies of the decay $B^0 \to \phi\gamma$ [2–7], which has similar quark-level transitions as the $B^0 \to \phi\mu^+\mu^-$ decay. The annihilation contributions to the $B^0 \to \phi\gamma$ branching fraction have been found to be of the order of 10^{-12} to 10^{-11} [2–4], depending on the factorization techniques. Contributions by new particles such as a Z' boson in the annihilation diagrams could be of the order of 10^{-9}–10^{-8} [2, 5], large enough to be observed by the LHCb detector. A recent study with soft-collinear effective theory indicates that the contribution from $\omega - \phi$ mixing could be three orders of magnitude larger than the pure annihilation contribution in the SM, increasing the branching fraction of the decay $B^0 \to \phi\gamma$ to $\mathcal{O}(10^{-9})$ [6]. The decay $B^0 \to \phi\gamma$ has not yet been observed, and the current upper limit on the branching fraction is 1.0×10^{-7} at a 90% confidence level set by the Belle collaboration [7].

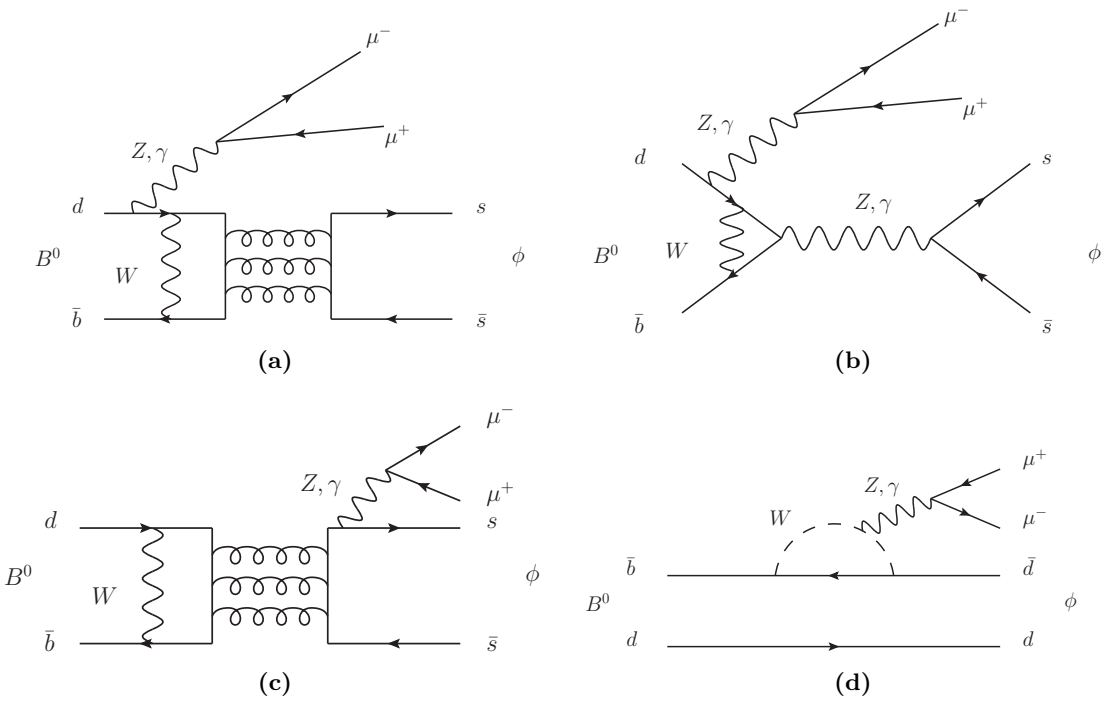

Figure 1. Standard Model Feynman diagrams for the decay $B^0 \to \phi\mu^+\mu^-$. (a), (b), (c) represent the weak annihilation contributions, while (d) represents the contribution from $\omega - \phi$ mixing.

Assuming a dominant $\omega - \phi$ contribution [6] and scaling the $B^0 \to \rho^0\mu^+\mu^-$ branching fraction measured by the LHCb experiment [8], the $B^0 \to \phi\mu^+\mu^-$ branching fraction is predicted to be between 10^{-11} and 10^{-10}. The decay $B^0 \to \phi\mu^+\mu^-$ has not yet been observed, but may be accessible at high luminosity flavour physics experiments such as the LHCb experiment and its upgrade, where it can be reconstructed with high efficiency.

This article presents a search for the decay $B^0 \to \phi\mu^+\mu^-$ performed using proton-proton (pp) collision data collected with the LHCb detector, corresponding to a total integrated luminosity of $9\,\text{fb}^{-1}$, comprising $3\,\text{fb}^{-1}$ collected at centre-of-mass energies of 7 and 8 TeV during 2011 and 2012 (denoted Run 1) and $6\,\text{fb}^{-1}$ collected at 13 TeV from 2015 to 2018 (denoted Run 2). The search is performed in the kinematically allowed range of q^2, the squared invariant mass of the dimuon system, excluding the ϕ region of 0.98–1.1 GeV^2/c^4, the J/ψ region of 8.0–11.0 GeV^2/c^4, and the $\psi(2S)$ region of 12.5–15.0 GeV^2/c^4. The decay $B_s^0 \to \phi\mu^+\mu^-$ is used as the normalization channel; its branching fraction in the same q^2 regions has already been measured by the LHCb experiment [9]. The more copious decay $B_s^0 \to J/\psi\phi$ with $J/\psi \to \mu^+\mu^-$ has identical final-state products and similar kinematic distributions as $B_{(s)}^0 \to \phi\mu^+\mu^-$ decays. A high purity sample of $B_s^0 \to J/\psi\phi$ decays is used to develop a multivariate event classifier and determine the mass model for nonresonant $B_{(s)}^0 \to \phi\mu^+\mu^-$ decays, where nonresonant refers to the $\mu^+\mu^-$ pair.

JHEP05(2022)067

2 Detector and simulation

The LHCb detector [10, 11] is a single-arm forward spectrometer covering the pseudorapidity range $2 < \eta < 5$, designed for the study of particles containing b or c quarks. The detector includes a high-precision tracking system consisting of a silicon-strip vertex detector surrounding the pp interaction region [12], a large-area silicon-strip detector located upstream of a dipole magnet with a bending power of about 4 Tm, and three stations of silicon-strip detectors and straw drift tubes [13, 14] placed downstream of the magnet. The tracking system provides a measurement of the momentum, p, of charged particles with a relative uncertainty that varies from 0.5% at low momentum to 1.0% at 200 GeV/c. The minimum distance of a track to a primary pp collision vertex (PV), the impact parameter (IP), is measured with a resolution of $(15 + 29/p_{\mathrm{T}})\,\mu$m, where p_{T} is the component of the momentum transverse to the beam, in GeV/c. Different types of charged hadrons are distinguished using information from two ring-imaging Cherenkov detectors [15]. Photons, electrons and hadrons are identified by a calorimeter system consisting of scintillating-pad and preshower detectors, an electromagnetic and a hadronic calorimeter. Muons are identified by a system composed of alternating layers of iron and multiwire proportional chambers [16].

The online event selection is performed by a trigger [17], consisting of a hardware stage, based on information from the calorimeter and muon systems, followed by a software stage, which applies a full event reconstruction. In the hardware stage, signal candidates are required to have at least one muon with p_{T} greater than 1 to 2 GeV/c or a pair of muons with the product of their p_{T} above 1 to 4 GeV$^2/c^2$, depending on the data-taking conditions. The software trigger requires a two-, three- or four-track secondary vertex with a significant displacement from any PV. At least one charged particle must have a p_{T} greater than 1 GeV/c and be inconsistent with originating from a PV. A multivariate algorithm [18] is used for the identification of secondary vertices consistent with the decay of a b hadron. The total trigger efficiency is 81%, where this quantity is defined as the number of simulated signal events that pass the full selection, including the trigger, divided by the number of signal events that pass all the section criteria, except the trigger requirements.

Samples of simulated decays are used to determine the trigger, reconstruction and selection efficiencies of the signal and control channels, as well as to estimate contamination from specific background processes. In the simulation, pp collisions are generated using Pythia [19] with a specific LHCb configuration [20]. Decays of unstable particles are described by EvtGen [21], in which final-state radiation is generated using Photos [22]. The interaction of the generated particles with the detector, and its response, are implemented using the Geant4 toolkit [23, 24] as described in ref. [25].

3 Candidate selection

The candidates of the $B^0_{(s)} \to \phi\mu^+\mu^-$ signal sample and the $B^0_s \to J/\psi\phi$ control sample are reconstructed by combining a pair of oppositely charged tracks, identified as muons, and a pair of oppositely charged tracks, identified as kaons. These tracks are required to be

JHEP05(2022)067

compatible with originating from a common vertex and have significant $\chi^2_{\rm IP}$ with respect to all primary interaction vertices, where $\chi^2_{\rm IP}$ is defined as the difference in the vertex-fit χ^2 of a given PV reconstructed with and without the track under consideration. The $B^0_{(s)}$ candidates must have a decay vertex significantly displaced from any PV and be compatible with originating from one of the PVs, considered as the $B^0_{(s)}$ production vertex. The angle between the vector connecting the production and decay vertices and the momentum of the $B^0_{(s)}$ candidate, θ, must satisfy $\cos\theta > 0.999$. The mass of the $K^+K^-\mu^+\mu^-$ combination is restricted to the range 5100–5800 MeV/c^2 and the invariant mass of the K^+K^- pair must be within 12 MeV/c^2 of the known ϕ mass [26]. The $B^0_{(s)} \to \phi\mu^+\mu^-$ signal candidates are selected in the q^2 range excluding the ϕ and charmonium regions, while the $B^0_s \to J/\psi\phi$ candidates are required to have a q^2 in the J/ψ region of 8.0–11.0 GeV$^2/c^4$.

There are two major sources of peaking background. The first consists of $B^0_s \to J/\psi\phi$ decays with a muon reconstructed as a kaon and a kaon as a muon. This background is suppressed by removing candidates that have a $K^\pm\mu^\mp$ mass in the J/ψ region, where a muon mass is assigned to any kaon candidate that satisfies strict criteria for muon selection. The second peaking background is due to $\Lambda^0_b \to pK^-\mu^+\mu^-$ decays with the proton misidentified as a kaon.[1] This source is suppressed by rejecting candidates in the Λ^0_b region of the $K^+K^-\mu^+\mu^-$ mass spectrum, where a proton mass is assigned to any kaon candidate that satisfies strict criteria for proton selection.

A boosted decision tree (BDT) [27, 28] classifier is employed to reduce the combinatorial background arising from random track combinations. The BDT input variables include the $\chi^2_{\rm IP}$ of all final state tracks and of the $B^0_{(s)}$ candidate, cosine of the angle θ, the fit χ^2 of the $B^0_{(s)}$ decay vertex and its displacement from the production vertex, the $B^0_{(s)}$ transverse momentum, the particle identification information of the final-state products, and the multiplicity and kinematic information of tracks consistent with the $B^0_{(s)}$ decay vertex but not associated with the $B^0_{(s)}$ candidate.

Separate BDT classifiers are trained for data taken in the Run 1 and Run 2 periods. The training of each BDT uses a data sample enriched with $B^0_s \to J/\psi\phi$ signal candidates, of which each event is assigned a weight for background subtraction using the *sPlot* technique [29] with the mass $m(K^+K^-\mu^+\mu^-)$ as the discriminating variable. The background sample used in the training consists of $K^+K^-\mu^+\mu^-$ combinations with invariant mass of the dimuon pair outside the J/ψ and $\psi(2S)$ mass regions, invariant mass of the dikaon pair within 50 MeV/c^2 of the known ϕ mass, and $m(K^+K^-\mu^+\mu^-)$ more than 200 MeV/c^2 above the known B^0_s mass [26]. This $m(K^+K^-\mu^+\mu^-)$ sideband is chosen to avoid overlapping the mass region used in the subsequent mass fit.

The BDT threshold is chosen to maximize the figure of merit for the decay $B^0 \to \phi\mu^+\mu^-$, defined as $\varepsilon/(\frac{a}{2} + \sqrt{B})$ [30]. Here ε is the signal efficiency of the BDT requirement, which is estimated using a data sample of $B^0_s \to J/\psi\phi$ candidates independent of the $B^0_s \to J/\psi\phi$ sample used for BDT training. The background yield, B, in the B^0 signal mass window of [5249, 5309] MeV/c^2 is estimated via interpolation between the lower sideband of [5170, 5249] MeV/c^2 and upper sideband of [5309, 5570] MeV/c^2. The targeted significance,

[1] The inclusion of charge-conjugate states is implied throughout.

JHEP05(2022)067

a, is set to 3. The same BDT requirement is used for the selection of $B^0 \to \phi\mu^+\mu^-$, $B_s^0 \to \phi\mu^+\mu^-$, and $B_s^0 \to J/\psi\phi$ decays. The distributions of the BDT input variables and the efficiency of the BDT requirement are found to be similar in the three channels according to the simulation. This ensures that the BDT classifier trained and optimized using the $B_s^0 \to J/\psi\phi$ control sample is also optimal for the $B_{(s)}^0 \to \phi\mu^+\mu^-$ channels. The BDT classifier rejects about 99% of the combinatorial background, while keeping about 80% of the signal and control channnel candidates.

The reconstruction and selection efficiencies needed for the branching fraction calculation are determined using simulated samples of $B^0 \to \phi\mu^+\mu^-$ and $B_s^0 \to \phi\mu^+\mu^-$ decays, which are generated using a phase-space model and an amplitude model with inputs from ref. [31]. The simulation is corrected for imperfect modeling of the particle identification performance, the track multiplicity, the distributions of transverse momentum, and vertex fit χ^2 of the $B_{(s)}^0$ mesons, using the $B_s^0 \to J/\psi\phi$ control sample from the data. The ratio of the average efficiencies for $B^0 \to \phi\mu^+\mu^-$ and $B_s^0 \to \phi\mu^+\mu^-$ decays with q^2 outside the ϕ and charmonium regions is evaluated to be $\varepsilon(B^0 \to \phi\mu^+\mu^-)/\varepsilon(B_s^0 \to \phi\mu^+\mu^-) = 0.999 \pm 0.009$ for Run 1 and 0.969 ± 0.007 for Run 2, respectively. Here, the uncertainties are due to limited size of the simulation samples.

4 Mass fits

The branching fraction of the nonresonant decay $B^0 \to \phi\mu^+\mu^-$ relative to that of the decay $B_s^0 \to \phi\mu^+\mu^-$ is estimated from a fit to the $K^+K^-\mu^+\mu^-$ mass distribution in a range that contains both the B^0 and B_s^0 signal peaks. The signal mass shape of the $B_{(s)}^0 \to \phi\mu^+\mu^-$ decays is partially determined using the $B_s^0 \to J/\psi\phi$ control sample. The $K^+K^-\mu^+\mu^-$ mass distribution of $B_s^0 \to J/\psi\phi$ candidates in the range 5100–5570 MeV/c^2 is shown in figure 2. An unbinned maximum-likelihood fit is performed to this distribution, separately for Run 1 and Run 2 data. The $B_s^0 \to J/\psi\phi$ candidates are reconstructed and selected in the same way as the nonresonant candidates, with no J/ψ mass constraint applied. The probability density function (PDF) for this fit is the sum of a $B_s^0 \to J/\psi\phi$ component, a $B^0 \to J/\psi K^+K^-$ component, and three background components. The $B_s^0 \to J/\psi\phi$ component is described by a double-sided Hypatia function [32], with tail parameters obtained from the fit. The $B^0 \to J/\psi K^+K^-$ component has the same shape as that of the $B_s^0 \to J/\psi\phi$ decay, and the difference of their mean values is constrained to the difference of the known B^0 and B_s^0 masses [26]. The $B^0 \to J/\psi K^+K^-$ yield is fixed to the estimate of 119 ± 19 for Run 1 (362 ± 51 for Run 2) obtained *a priori* from another mass fit where the invariant mass of the $B_s^0 \to J/\psi\phi$ candidates is computed with a J/ψ mass constraint applied on the dimuon pair.

The combinatorial background for $B_s^0 \to J/\psi\phi$ is described by an exponential function. The residual background from $\Lambda_b^0 \to J/\psi pK^-$ decays passing the dedicated veto is described by a template obtained from simulation. The $\Lambda_b^0 \to J/\psi pK^-$ yield is fixed to the estimate of 253 ± 53 for Run 1 (1251 ± 172 for Run 2), which is obtained *a priori* by changing the mass hypothesis of one kaon to a proton and fitting the $pK^-\mu^+\mu^-$ mass distribution, following the procedure described in refs. [33, 34]. The partially reconstructed

JHEP05(2022)067

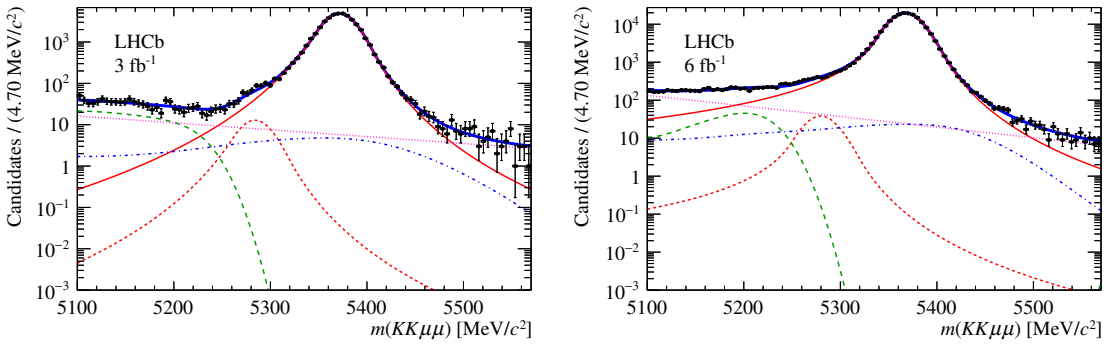

Figure 2. The $K^+K^-\mu^+\mu^-$ mass distributions of selected $B^0_s \to J/\psi\phi$ candidates in (left) Run 1 and (right) Run 2 data, with the fit projections overlaid. The red solid line is $B^0_s \to J/\psi\phi$ signal, the red dashed line is $B^0 \to J/\psi K^+K^-$ signal, the green dashed line is the partially reconstructed background component, the violet dotted line is the combinatorial background component, and the blue dash-dot line is the $\Lambda^0_b \to J/\psi pK^-$ background component.

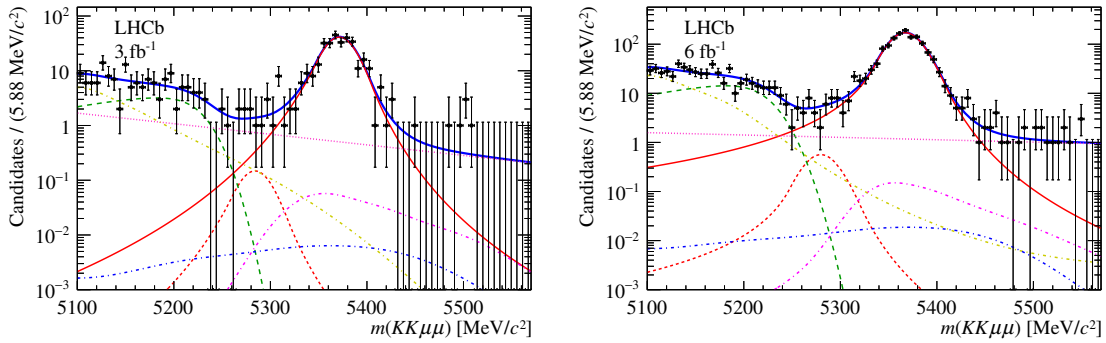

Figure 3. The $K^+K^-\mu^+\mu^-$ mass distributions of selected nonresonant $B^0_{(s)} \to \phi\mu^+\mu^-$ candidates in (left) Run 1 and (right) Run 2 data. The red solid line is $B^0_s \to \phi\mu^+\mu^-$ signal, the red dashed line is $B^0 \to \phi\mu^+\mu^-$ signal, the green dashed line is the partially reconstructed background component, the violet dotted line is the combinatorial background component, the blue dash-dot line is the $\Lambda^0_b \to pK^-\mu^+\mu^-$ background component, the violet dash-dot line is the $B^0 \to K^{*0}(\to K^+\pi^-)\mu^+\mu^-$ background component, and the orange dash-dot line is the $B^0_s \to D^-_s(\to \phi\mu^-\bar{\nu})\mu^+\nu$ background component.

background mainly arises from B-meson decays to final states with a π^0, and is modelled by an Argus function [35] convolved with a Gaussian resolution function with a width equal to that of the signal Hypatia function. The endpoint of the Argus function is fixed to the mean of the B^0_s mass peak minus the π^0 mass [26]. The fit projections of the $K^+K^-\mu^+\mu^-$ mass distributions of selected $B^0_s \to J/\psi\phi$ candidates are shown in figure 2 and are in good agreement with data.

A simultaneous unbinned maximum-likelihood fit is performed to the $K^+K^-\mu^+\mu^-$ mass distributions of selected $B^0_{(s)} \to \phi\mu^+\mu^-$ candidates, shown in figure 3, in the Run 1 and Run 2 data samples. The fit range is 5100–5570 MeV/c^2. The fit model detailed below keeps the same form for Run 1 and Run 2, while the fit parameters can take different values

JHEP05(2022)067

for the two periods except for the parameter of interest, the branching fraction ratio in the q^2 range excluding the ϕ and charmonium regions,

$$\mathcal{R} = \frac{\mathcal{B}(B^0 \to \phi\mu^+\mu^-)}{\mathcal{B}(B_s^0 \to \phi\mu^+\mu^-)} , \tag{4.1}$$

which is required to be common for Run 1 and Run 2. The fit PDF includes the $B^0 \to \phi\mu^+\mu^-$ and $B_s^0 \to \phi\mu^+\mu^-$ components; a combinatorial background component; several additional background components from specific B-meson decays: $B^0 \to K^{*0}(\to K^+\pi^-)\mu^+\mu^-$, $\Lambda_b^0 \to pK^-\mu^+\mu^-$, $B_s^0 \to D_s^-(\to \phi\mu^-\bar{\nu})\mu^+\nu$; and an inclusive partially reconstructed background component.

As in the $B_s^0 \to J/\psi\phi$ case, the $B_s^0 \to \phi\mu^+\mu^-$ component is described by a double-sided Hypatia function and its tail parameters are fixed to the values obtained in the $B_s^0 \to J/\psi\phi$ fit. The width, mean, and yield ($N_{B_s^0}$) are allowed to vary in the fit. The $B^0 \to \phi\mu^+\mu^-$ component is described by the same double-sided Hypatia function as for B_s^0 decays shifted by the difference of the known B^0 and B_s^0 masses. The branching fraction ratio $\mathcal{R}$ is included as a free fit parameter. The $B^0 \to \phi\mu^+\mu^-$ yield (N_{B^0}) is expressed in terms of $N_{B_s^0}$ and $\mathcal{R}$ according to

$$N_{B^0} = \frac{\mathcal{R}}{f_s/f_d} \times \frac{\varepsilon(B^0 \to \phi\mu^+\mu^-)}{\varepsilon(B_s^0 \to \phi\mu^+\mu^-)} \times N_{B_s^0} . \tag{4.2}$$

Here $\varepsilon(B^0 \to \phi\mu^+\mu^-)/\varepsilon(B_s^0 \to \phi\mu^+\mu^-)$ is the efficiency ratio given in section 3, and f_s/f_d is the ratio of the production fractions of B_s^0 and B^0 mesons in the LHCb detector acceptance in pp collisions, which has been measured to be 0.2390 ± 0.0076 at 7 TeV, 0.2385 ± 0.0075 at 8 TeV, and 0.2539 ± 0.0079 at 13 TeV [36]. The factors f_s/f_d and $\varepsilon(B^0 \to \phi\mu^+\mu^-)/\varepsilon(B_s^0 \to \phi\mu^+\mu^-)$ are fixed to their central values in the baseline fit, and their uncertainties are taken into account in the evaluation of the systematic uncertainties of the $\mathcal{R}$ measurement.

As in the $B_s^0 \to J/\psi\phi$ case, the combinatorial background for $B_{(s)}^0 \to \phi\mu^+\mu^-$ is described by an exponential function, the inclusive partially reconstructed background is modelled by an Argus function convolved with a Gaussian resolution function, and the Argus endpoint is set to the mean of the B_s^0 mass peak minus the π^0 mass.

Three sources of specific physics background are accounted for in the $B_{(s)}^0 \to \phi\mu^+\mu^-$ mass fit, $B^0 \to K^{*0}(\to K^+\pi^-)\mu^+\mu^-$ decays with the pion misidentified as a kaon, residual $\Lambda_b^0 \to pK^-\mu^+\mu^-$ decays with the proton misidentified as a kaon and $B_s^0 \to D_s^-(\to \phi\mu^-\bar{\nu})\mu^+\nu$ decays with the two neutrinos undetected. Their mass models are implemented as templates obtained from corrected simulation. The yields are determined relative to the $B_s^0 \to \phi\mu^+\mu^-$ yield, using the known branching fractions and the efficiencies relative to that of $B_s^0 \to \phi\mu^+\mu^-$ given in table 1. The obtained yields are $N_{B^0 \to K^{*0}\mu^+\mu^-} = 1.21 \pm 0.23$, $N_{\Lambda_b^0 \to pK^-\mu^+\mu^-} = 0.29 \pm 0.12$, and $N_{B_s^0 \to D_s^-\mu^+\nu} = 52 \pm 17$ for Run 1 (2.87 ± 0.51, 0.87 ± 0.35, and 240 ± 77 for Run 2). The central values of these yields are used in the baseline fit and their uncertainties are considered as sources of systematic uncertainties for the $\mathcal{R}$ estimate.

JHEP05(2022)067

Process	$\varepsilon_{\rm bkg}/\varepsilon_{B_s^0}$ [$\times 10^{-3}$]	
	Run 1	Run 2
$B^0 \to K^{*0}\mu^+\mu^-$	0.671 ± 0.041	0.344 ± 0.018
$\Lambda_b^0 \to pK^-\mu^+\mu^-$	0.717 ± 0.033	0.469 ± 0.016
$B_s^0 \to D_s^-\mu^+\nu$	0.298 ± 0.015	0.299 ± 0.008

Table 1. Efficiencies of background decay processes relative to that of the decay $B_s^0 \to \phi\mu^+\mu^-$ evaluated using simulated samples. The uncertainties are due to limited sizes of these samples.

The $B_s^0 \to \phi\mu^+\mu^-$ signal yields are 302 ± 19 for Run 1 and 1389 ± 41 for Run 2. The fit projections are shown in figure 3, and there is no visible $B^0 \to \phi\mu^+\mu^-$ signal contribution. Thus the upper limits on its relative and absolute branching fractions are calculated in section 6.

5 Systematic uncertainties

Due to the identical decay products and similar event topology of the $B^0 \to \phi\mu^+\mu^-$ and $B_s^0 \to \phi\mu^+\mu^-$ decays, systematic uncertainties associated with the evaluation of the efficiency cancel in the branching fraction ratio $\mathcal{R}$. The remaining systematic uncertainties, including additive ones associated with the yield estimation and multiplicative ones propagated from the scaling factors involved in the calculation of $\mathcal{R}$, are summarized in table 2 and discussed below.

The dominant systematic uncertainty is associated with modelling the mass shapes of the signals. This effect has been studied by fitting the data using an alternative model, generating a large number of samples according to the obtained new model, and fitting each pseudoexperiments with both the baseline and alternative model. The mean change in $\mathcal{R}$ is assigned as a systematic uncertainty. For $B_{(s)}^0 \to \phi\mu^+\mu^-$ decays, replacing the double-sided Hypatia function with the sum of two double-sided Crystal Ball functions leads to an uncertainty of 0.39×10^{-3} on $\mathcal{R}$. For the inclusive partially reconstructed background, changing the resolution model from a Gaussian to a Hypatia function causes an uncertainty of 0.15×10^{-3}.

Another major contribution to the systematic uncertainty is associated with the specific background from $B_s^0 \to D_s^-(\to \phi\mu^-\bar{\nu})\mu^+\nu$ decays with missing neutrinos, which lies under the inclusive partially reconstructed background in the $K^+K^-\mu^+\mu^-$ mass spectrum. The shape of this background is described by a template obtained from simulation. The uncertainty due to the finite size of the simulated sample is evaluated using a bootstrapping technique [37]. A large number of new samples of the same size as the original simulation sample are formed by randomly cloning events from the original sample. The standard deviation on the results of $\mathcal{R}$ obtained using the new samples is taken as a systematic uncertainty, which is estimated to be 0.13×10^{-3}. In the baseline fit, the yield of the $B_s^0 \to D_s^-\mu^+\nu$ background is fixed to the central value of the estimate given in section 4.

JHEP05(2022)067

Additive uncertainties	Value [$\times 10^{-3}$]
Fit bias	0.09
Signal model	0.39
Partial background	0.15
Yield of $B^0 \to J/\psi K^+ K^-$	0.09
Yield of $\Lambda_b^0 \to J/\psi p K^-$	0.07
Yield of $B^0 \to K^{*0}\mu^+\mu^-$	0.01
Yield of $\Lambda_b^0 \to pK^-\mu^+\mu^-$	0.03
Yield of $B_s^0 \to D_s^-\mu^+\nu$	0.27
Shape of $B^0 \to K^{*0}\mu^+\mu^-$	0.01
Shape of $\Lambda_b^0 \to pK^-\mu^+\mu^-$	0.00
Shape of $B_s^0 \to D_s^-\mu^+\nu$	0.13
Total	**0.54**
Multiplicative uncertainties	Value [%]
f_s/f_d	3.1
$\varepsilon_{B^0}/\varepsilon_{B_s^0}$	0.8
Total	**3.2**

Table 2. Systematic uncertainties on the measurement of $\mathcal{R}$ for additive and multiplicative sources.

Changing this yield by ± 1 standard deviations and repeating the $B^0_{(s)} \to \phi\mu^+\mu^-$ mass fit, the maximum change of $\mathcal{R}$ is 0.27×10^{-3}, which is assigned as a systematic uncertainty.

The systematic uncertainties associated with other specific background components in the $B^0_{(s)} \to \phi\mu^+\mu^-$ sample are also studied and found to be small. Changing the fixed yield of the $B^0 \to J/\psi K^+K^-$ ($\Lambda_b^0 \to J/\psi p K^-$) component in the $B_s^0 \to J/\psi\phi$ fit by ± 1 standard deviations leads to a systematic uncertainty of 0.09×10^{-3} (0.07×10^{-3}) on $\mathcal{R}$. The average bias in $\mathcal{R}$ due to the maximum likelihood fit procedure is evaluated to be 0.09×10^{-3} using pseudoexperiments. Summing the contributions discussed above in quadrature leads to a total additive systematic uncertainty of $\sigma_{\text{add}} = 0.54 \times 10^{-3}$.

As can be seen in eq. 4.2, the estimate of $\mathcal{R}$ is proportional to the production fraction ratio f_s/f_d and the efficiency ratio $\varepsilon_{B_s^0}/\varepsilon_{B^0}$. In the baseline fit, these scaling factors are fixed to their central values obtained *a priori*. The relative uncertainties of the luminosity-averaged values of f_s/f_d and $\varepsilon_{B^0}/\varepsilon_{B_s^0}$ are 3.1% and 0.8%, respectively, which are propagated to $\mathcal{R}$ as multiplicative systematic uncertainties. The combined multiplicative uncertainty on $\mathcal{R}$ is $k = 3.2\%$. The total systematic uncertainty on $\mathcal{R}$ can be written as

$$\sigma(\mathcal{R}) = \sqrt{\sigma^2_{\text{add}} + (k \times \mathcal{R})^2}\,. \tag{5.1}$$

JHEP05(2022)067

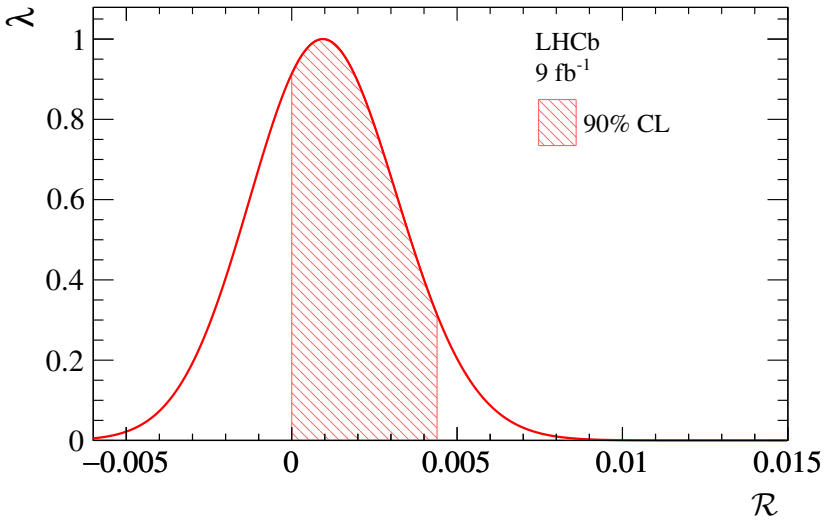

Figure 4. Smeared profile likelihood ratio curve from the simultaneous fit to the Run 1 and Run 2 data samples. The red shaded area indicates the 90% crediblity interval of $\mathcal{R}$.

6 Results

Since no significant signal of the decay $B^0 \to \phi\mu^+\mu^-$ is observed, an upper limit on the branching fraction ratio $\mathcal{R}$ is determined using the profile likelihood method [38, 39]. The profile likelihood ratio as a function of $\mathcal{R}$, denoted $\lambda_0(\mathcal{R})$, is defined as the ratio of the maximum likelihood value for a given value of the parameter of interest, $\mathcal{R}$, to the global maximum likelihood value. In order to incorporate the systematic uncertainties, a smeared profile likelihood ratio function is defined as

$$\lambda(\mathcal{R}) = \lambda_0(\mathcal{R}') \otimes G(\mathcal{R} - \mathcal{R}'; 0, \sigma(\mathcal{R}')) \,, \tag{6.1}$$

where $\lambda_0(\mathcal{R}')$ is convolved with a Gaussian function, which has a zero mean and a width equal to the total systematic uncertainty given in eq. 5.1.

Figure 4 shows the smeared likelihood function $\lambda(\mathcal{R})$ obtained from the simultaneous fit to the Run 1 and Run 2 data samples, where the shaded area starting at $\mathcal{R} = 0$ defines a 90% credibility interval obtained using a prior function that is uniform in the physical region $\mathcal{R} > 0$. The right boundary of this interval gives the upper limit on $\mathcal{R}$

$$\mathcal{R} < 4.4 \times 10^{-3} \text{ at a 90\% crediblity level (CL)} \,.$$

The limit on $\mathcal{R}$ can be converted into a limit on the branching fraction $\mathcal{B}(B^0 \to \phi\mu^+\mu^-)$ using a previous measurement of $\mathcal{B}(B_s^0 \to \phi\mu^+\mu^-)$ in the same q^2 intervals. The LHCb collaboration reported $\mathcal{B}(B_s^0 \to \phi\mu^+\mu^-) = (8.14 \pm 0.21\,(\text{stat}) \pm 0.16\,(\text{syst}) \pm 0.03\,(\text{extrap}) \pm 0.39\,(B_s^0 \to J/\psi\phi)) \times 10^{-7}$ [9] in the full q^2 range without the resonant vetoes, where the third uncertainty is associated with the extrapolation used to recover the vetoed ϕ and charmonium regions in the q^2 spectrum. Using the extrapolation factor of $F_e^s = (65.47 \pm 0.27)\%$ given in ref. [9], the branching fraction excluding the ϕ and charmonium

JHEP05(2022)067

regions is $\mathcal{B}(B_s^0 \to \phi\mu^+\mu^-) = (5.33 \pm 0.14\,(\text{stat}) \pm 0.10\,(\text{syst}) \pm 0.25\,(B_s^0 \to J/\psi\phi)) \times 10^{-7}$. Among these uncertainties, the contributions from the $B_s^0 \to \phi\mu^+\mu^-$ yield and f_s/f_d ratio are almost completely anticorrelated with the corresponding uncertainties on $\mathcal{R}$. Taking this correlation into account, the net uncertainty propagated from $\mathcal{B}(B_s^0 \to \phi\mu^+\mu^-)$ to $\mathcal{B}(B^0 \to \phi\mu^+\mu^-)$ is found to be negligible. A limit on $\mathcal{B}(B^0 \to \phi\mu^+\mu^-)$ in the q^2 range excluding the ϕ and charmonium regions is set to be 2.3×10^{-9} at a 90% CL.

The fraction of $B^0 \to \phi\mu^+\mu^-$ decays within the considered q^2 regions is calculated to be $F_e^d = (73.2 \pm 0.1)\%$ with a phase-space decay model. Using this fraction, the limits on the total branching fractions in the full q^2 range is determined to be

$$\mathcal{B}(B^0 \to \phi\mu^+\mu^-) < 3.2 \times 10^{-9} \text{ at a } 90\% \text{ CL} .$$

The observed limit on $\mathcal{B}(B^0 \to \phi\mu^+\mu^-)$ is consistent with the expected limit, which is evaluated to be 3.1×10^{-9} at a 90% CL using pseudoexperiments generated under the assumption of zero $B^0 \to \phi\mu^+\mu^-$ signal. Alternative models are used to check the dependency of the result on the $B^0 \to \phi\mu^+\mu^-$ decay model. The phase-space model is replaced by a model that has the same q^2 and angular distributions as in $B_s^0 \to \phi\mu^+\mu^-$ decays or a model that has the same q^2 distribution as in $B_s^0 \to \phi\mu^+\mu^-$ decays but a flat angular distribution. The evaluated upper limits on $\mathcal{B}(B^0 \to \phi\mu^+\mu^-)$ increase by less than 5% and 15% in the q^2 range, excluding the ϕ and charmonium resonances, and in the full q^2 range, respectively.

7 Conclusion

This article presents the first search for the decay $B^0 \to \phi\mu^+\mu^-$, performed using pp collision data at centre-of-mass energies of 7, 8, and 13 TeV collected by the LHCb experiment, corresponding to an integrated luminosity of $9\,\text{fb}^{-1}$. No statistically significant excess of the decay $B^0 \to \phi\mu^+\mu^-$ above the background is observed. An upper limit on its branching fraction excluding the ϕ and charmonium regions in the dimuon spectrum relative to that of the decay $B_s^0 \to \phi\mu^+\mu^-$ is determined to be 4.4×10^{-3} at a 90% CL. Assuming a phase-space decay model for the decay $B^0 \to \phi\mu^+\mu^-$ and using the LHCb measurement of $\mathcal{B}(B_s^0 \to \phi\mu^+\mu^-)$, an upper limit on $\mathcal{B}(B^0 \to \phi\mu^+\mu^-)$ in the full q^2 range is set to be 3.2×10^{-9} at a 90% CL, which is compatible with the SM prediction.

Acknowledgments

We express our gratitude to our colleagues in the CERN accelerator departments for the excellent performance of the LHC. We thank the technical and administrative staff at the LHCb institutes. We acknowledge support from CERN and from the national agencies: CAPES, CNPq, FAPERJ and FINEP (Brazil); MOST and NSFC (China); CNRS/IN2P3 (France); BMBF, DFG and MPG (Germany); INFN (Italy); NWO (Netherlands); MNiSW and NCN (Poland); MEN/IFA (Romania); MSHE (Russia); MICINN (Spain); SNSF and SER (Switzerland); NASU (Ukraine); STFC (United Kingdom); DOE NP and NSF (USA). We acknowledge the computing resources that are provided by CERN, IN2P3 (France), KIT

JHEP05(2022)067

and DESY (Germany), INFN (Italy), SURF (Netherlands), PIC (Spain), GridPP (United Kingdom), RRCKI and Yandex LLC (Russia), CSCS (Switzerland), IFIN-HH (Romania), CBPF (Brazil), PL-GRID (Poland) and NERSC (USA). We are indebted to the communities behind the multiple open-source software packages on which we depend. Individual groups or members have received support from ARC and ARDC (Australia); AvH Foundation (Germany); EPLANET, Marie Skłodowska-Curie Actions and ERC (European Union); A*MIDEX, ANR, IPhU and Labex P2IO, and Région Auvergne-Rhône-Alpes (France); Key Research Program of Frontier Sciences of CAS, CAS PIFI, CAS CCEPP, Fundamental Research Funds for the Central Universities, and Sci. & Tech. Program of Guangzhou (China); RFBR, RSF and Yandex LLC (Russia); GVA, XuntaGal and GENCAT (Spain); the Leverhulme Trust, the Royal Society and UKRI (United Kingdom).

References

[1] A. Kuznetsova and A. Parkhomenko, *Annihilation-Type Semileptonic B-Meson Decays*, *EPJ Web Conf.* **158** (2017) 03003 [INSPIRE].

[2] X.-q. Li, G.-r. Lu, R.-m. Wang and Y.D. Yang, *The Rare $\bar{B}_d^0 \to \phi\gamma$ decays in standard model and as a probe of R parity violation*, *Eur. Phys. J. C* **36** (2004) 97 [hep-ph/0305283] [INSPIRE].

[3] Y. Li and C.-D. Lu, *Annihilation Type Radiative Decays of B Meson in Perturbative QCD Approach*, *Phys. Rev. D* **74** (2006) 097502 [hep-ph/0605220] [INSPIRE].

[4] C.-D. Lu, Y.-L. Shen and W. Wang, *Role of electromagnetic dipole operator in the electroweak penguin dominated vector meson decays of B meson*, *Chin. Phys. Lett.* **23** (2006) 2684 [hep-ph/0606092] [INSPIRE].

[5] J. Hua, C.S. Kim and Y. Li, *Annihilation-Type Charmless Radiative Decays of B Meson in Non-universal Z' Model*, *Eur. Phys. J. C* **69** (2010) 139 [arXiv:1002.2531] [INSPIRE].

[6] H. Deng, J. Gao, L.-Y. Li, C.-D. Lü, Y.-L. Shen and C.-X. Yu, *Study on pure annihilation type $B \to V\gamma$ decays*, *Phys. Rev. D* **103** (2021) 076004 [arXiv:2101.01344] [INSPIRE].

[7] Belle collaboration, *Search for the decay $B^0 \to \phi\gamma$*, *Phys. Rev. D* **93** (2016) 111101 [arXiv:1603.06546] [INSPIRE].

[8] LHCb collaboration, *Study of the rare B_s^0 and B^0 decays into the $\pi^+\pi^-\mu^+\mu^-$ final state*, *Phys. Lett. B* **743** (2015) 46 [arXiv:1412.6433] [INSPIRE].

[9] LHCb collaboration, *Branching Fraction Measurements of the Rare $B_s^0 \to \phi\mu^+\mu^-$ and $B_s^0 \to f_2'(1525)\mu^+\mu^-$ decays*, *Phys. Rev. Lett.* **127** (2021) 151801 [arXiv:2105.14007] [INSPIRE].

[10] LHCb collaboration, *The LHCb Detector at the LHC*, 2008 *JINST* **3** S08005 [INSPIRE].

[11] LHCb collaboration, *LHCb Detector Performance*, *Int. J. Mod. Phys. A* **30** (2015) 1530022 [arXiv:1412.6352] [INSPIRE].

JHEP05(2022)067

[12] R. Aaij et al., *Performance of the LHCb Vertex Locator*, 2014 *JINST* **9** P09007 [arXiv:1405.7808] [INSPIRE].

[13] R. Arink et al.,, *Performance of the LHCb Outer Tracker*, 2014 *JINST* **9** P01002 [arXiv:1311.3893] [INSPIRE].

[14] P. d'Argent et al., *Improved performance of the LHCb Outer Tracker in LHC Run 2*, 2017 *JINST* **12** P11016 [arXiv:1708.00819] [INSPIRE].

[15] M. Adinolfi et al., *Performance of the LHCb RICH detector at the LHC*, *Eur. Phys. J. C* **73** (2013) 2431 [arXiv:1211.6759] [INSPIRE].

[16] A.A. Alves, Jr. et al., *Performance of the LHCb muon system*, 2013 *JINST* **8** P02022 [arXiv:1211.1346] [INSPIRE].

[17] R. Aaij et al., *The LHCb Trigger and its Performance in 2011*, 2013 *JINST* **8** P04022 [arXiv:1211.3055] [INSPIRE].

[18] V.V. Gligorov and M. Williams, *Efficient, reliable and fast high-level triggering using a bonsai boosted decision tree*, 2013 *JINST* **8** P02013 [arXiv:1210.6861] [INSPIRE].

[19] T. Sjöstrand, S. Mrenna and P.Z. Skands, *A Brief Introduction to PYTHIA 8.1*, *Comput. Phys. Commun.* **178** (2008) 852 [arXiv:0710.3820] [INSPIRE].

[20] I. Belyaev et al., *Handling of the generation of primary events in Gauss, the LHCb simulation framework*, *J. Phys. Conf. Ser.* **331** (2011) 032047 [INSPIRE].

[21] D.J. Lange, *The EvtGen particle decay simulation package*, *Nucl. Instrum. Meth. A* **462** (2001) 152 [INSPIRE].

[22] N. Davidson, T. Przedzinski and Z. Was, *PHOTOS interface in C++: Technical and Physics Documentation*, *Comput. Phys. Commun.* **199** (2016) 86 [arXiv:1011.0937] [INSPIRE].

[23] Geant4 collaboration, *Geant4 developments and applications*, *IEEE Trans. Nucl. Sci.* **53** (2006) 270.

[24] GEANT4 collaboration, *GEANT4–a simulation toolkit*, *Nucl. Instrum. Meth. A* **506** (2003) 250 [INSPIRE].

[25] M. Clemencic et al., *The LHCb simulation application, Gauss: Design, evolution and experience*, *J. Phys. Conf. Ser.* **331** (2011) 032023 [INSPIRE].

[26] Particle Data Group collaboration, *Review of Particle Physics*, *PTEP* **2020** (2020) 083C01 [INSPIRE].

[27] L. Breiman, J.H. Friedman, R.A. Olshen and C.J. Stone, *Classification and regression trees*, Wadsworth international group, Belmont, California, U.S.A. (1984).

[28] Y. Freund and R. E. Schapire, *A decision-theoretic generalization of on-line learning and an application to boosting*, *J. Comput. Syst. Sci.* **55** (1997) 119.

[29] M. Pivk and F.R. Le Diberder, *SPlot: A Statistical tool to unfold data distributions*, *Nucl. Instrum. Meth. A* **555** (2005) 356 [physics/0402083] [INSPIRE].

[30] G. Punzi, *Sensitivity of searches for new signals and its optimization*, *eConf* **C 030908** (2003) MODT002 [physics/0308063] [INSPIRE].

[31] P. Ball and R. Zwicky, $B_{d,s} \to \rho, \omega, K^*, \phi$ *decay form-factors from light-cone sum rules revisited*, *Phys. Rev. D* **71** (2005) 014029 [hep-ph/0412079] [INSPIRE].

JHEP05(2022)067

[32] D. Martínez Santos and F. Dupertuis, *Mass distributions marginalized over per-event errors*, *Nucl. Instrum. Meth. A* **764** (2014) 150 [arXiv:1312.5000] [INSPIRE].

[33] LHCb collaboration, *Updated measurement of time-dependent CP-violating observables in $B_s^0 \to J/\psi K^+K^-$ decays*, *Eur. Phys. J. C* **79** (2019) 706 [*Erratum ibid.* **80** (2020) 601] [arXiv:1906.08356] [INSPIRE].

[34] LHCb collaboration, *Search for the rare decay $B^0 \to J/\psi\phi$*, *Chin. Phys. C* **45** (2021) 043001 [arXiv:2011.06847] [INSPIRE].

[35] W. Verkerke and D.P. Kirkby, *The RooFit toolkit for data modeling*, *eConf* **C 0303241** (2003) MOLT007 [physics/0306116] [INSPIRE].

[36] LHCb collaboration, *Precise measurement of the f_s/f_d ratio of fragmentation fractions and of B_s^0 decay branching fractions*, *Phys. Rev. D* **104** (2021) 032005 [arXiv:2103.06810] [INSPIRE].

[37] B. Efron, *Bootstrap methods: Another look at the jackknife*, *Ann. Statist.* **7** (1979) 1.

[38] G. Cowan, K. Cranmer, E. Gross and O. Vitells, *Asymptotic formulae for likelihood-based tests of new physics*, *Eur. Phys. J. C* **71** (2011) 1554 [*Erratum ibid.* **73** (2013) 2501] [arXiv:1007.1727] [INSPIRE].

[39] RooStats Team collaboration, *RooStats for Searches*, in *PHYSTAT 2011*, pp. 199–208, CERN, Geneva, Switzerland (2011), [arXiv:1203.1547] [INSPIRE].

JHEP05(2022)067

The LHCb collaboration

R. Aaij,[32] A.S.W. Abdelmotteleb,[56] C. Abellán Beteta,[50] F. Abudinén,[56] T. Ackernley,[60] B. Adeva,[46] M. Adinolfi,[54] H. Afsharnia,[9] C. Agapopoulou,[13] C.A. Aidala,[87] S. Aiola,[25] Z. Ajaltouni,[9] S. Akar,[65] J. Albrecht,[15] F. Alessio,[48] M. Alexander,[59] A. Alfonso Albero,[45] Z. Aliouche,[62] G. Alkhazov,[38] P. Alvarez Cartelle,[55] S. Amato,[2] J.L. Amey,[54] Y. Amhis,[11] L. An,[48] L. Anderlini,[22] M. Andersson,[50] A. Andreianov,[38] M. Andreotti,[21] D. Ao,[6] F. Archilli,[17] A. Artamonov,[44] M. Artuso,[68] K. Arzymatov,[42] E. Aslanides,[10] M. Atzeni,[50] B. Audurier,[12] S. Bachmann,[17] M. Bachmayer,[49] J.J. Back,[56] P. Baladron Rodriguez,[46] V. Balagura,[12] W. Baldini,[21] J. Baptista de Souza Leite,[1] M. Barbetti,[22,h] R.J. Barlow,[62] S. Barsuk,[11] W. Barter,[61] M. Bartolini,[55] F. Baryshnikov,[83] J.M. Basels,[14] G. Bassi,[29] B. Batsukh,[4] A. Battig,[15] A. Bay,[49] A. Beck,[56] M. Becker,[15] F. Bedeschi,[29] I. Bediaga,[1] A. Beiter,[68] V. Belavin,[42] S. Belin,[27] V. Bellee,[50] K. Belous,[44] I. Belov,[40] I. Belyaev,[41] G. Bencivenni,[23] E. Ben-Haim,[13] A. Berezhnoy,[40] R. Bernet,[50] D. Berninghoff,[17] H.C. Bernstein,[68] C. Bertella,[62] A. Bertolin,[28] C. Betancourt,[50] F. Betti,[48] Ia. Bezshyiko,[50] S. Bhasin,[54] J. Bhom,[35] L. Bian,[73] M.S. Bieker,[15] N.V. Biesuz,[21] S. Bifani,[53] P. Billoir,[13] A. Biolchini,[32] M. Birch,[61] F.C.R. Bishop,[55] A. Bitadze,[62] A. Bizzeti,[22,l] M. Bjørn,[63] M.P. Blago,[55] T. Blake,[56] F. Blanc,[49] S. Blusk,[68] D. Bobulska,[59] J.A. Boelhauve,[15] O. Boente Garcia,[46] T. Boettcher,[65] A. Boldyrev,[82] A. Bondar,[43] N. Bondar,[38,48] S. Borghi,[62] M. Borisyak,[42] M. Borsato,[17] J.T. Borsuk,[35] S.A. Bouchiba,[49] T.J.V. Bowcock,[60,48] A. Boyer,[48] C. Bozzi,[21] M.J. Bradley,[61] S. Braun,[66] A. Brea Rodriguez,[46] J. Brodzicka,[35] A. Brossa Gonzalo,[56] D. Brundu,[27] A. Buonaura,[50] L. Buonincontri,[28] A.T. Burke,[62] C. Burr,[48] A. Bursche,[72] A. Butkevich,[39] J.S. Butter,[32] J. Buytaert,[48] W. Byczynski,[48] S. Cadeddu,[27] H. Cai,[73] R. Calabrese,[21,g] L. Calefice,[15,13] S. Cali,[23] R. Calladine,[53] M. Calvi,[26,k] M. Calvo Gomez,[85] P. Camargo Magalhaes,[54] P. Campana,[23] A.F. Campoverde Quezada,[6] S. Capelli,[26,k] L. Capriotti,[20,e] A. Carbone,[20,e] G. Carboni,[31,q] R. Cardinale,[24,i] A. Cardini,[27] I. Carli,[4] P. Carniti,[26,k] L. Carus,[14] K. Carvalho Akiba,[32] A. Casais Vidal,[46] R. Caspary,[17] G. Casse,[60] M. Cattaneo,[48] G. Cavallero,[48] S. Celani,[49] J. Cerasoli,[10] D. Cervenkov,[63] A.J. Chadwick,[60] M.G. Chapman,[54] M. Charles,[13] Ph. Charpentier,[48] C.A. Chavez Barajas,[60] M. Chefdeville,[8] C. Chen,[3] S. Chen,[4] A. Chernov,[35] V. Chobanova,[46] S. Cholak,[49] M. Chrzaszcz,[35] A. Chubykin,[38] V. Chulikov,[38] P. Ciambrone,[23] M.F. Cicala,[56] X. Cid Vidal,[46] G. Ciezarek,[48] P.E.L. Clarke,[58] M. Clemencic,[48] H.V. Cliff,[55] J. Closier,[48] J.L. Cobbledick,[62] V. Coco,[48] J.A.B. Coelho,[11] J. Cogan,[10] E. Cogneras,[9] L. Cojocariu,[37] P. Collins,[48] T. Colombo,[48] L. Congedo,[19,d] A. Contu,[27] N. Cooke,[53] G. Coombs,[59] I. Corredoira ,[46] G. Corti,[48] C.M. Costa Sobral,[56] B. Couturier,[48] D.C. Craik,[64] J. Crkovská,[67] M. Cruz Torres,[1] R. Currie,[58] C.L. Da Silva,[67] S. Dadabaev,[83] L. Dai,[71] E. Dall'Occo,[15] J. Dalseno,[46] C. D'Ambrosio,[48] A. Danilina,[41] P. d'Argent,[48] A. Dashkina,[83] J.E. Davies,[62] A. Davis,[62] O. De Aguiar Francisco,[62] K. De Bruyn,[79] S. De Capua,[62] M. De Cian,[49] E. De Lucia,[23] J.M. De Miranda,[1] L. De Paula,[2] M. De Serio,[19,d] D. De Simone,[50] P. De Simone,[23] F. De Vellis,[15] J.A. de Vries,[80] C.T. Dean,[67] F. Debernardis,[19,d] D. Decamp,[8] V. Dedu,[10] L. Del Buono,[13] B. Delaney,[55] H.-P. Dembinski,[15] V. Denysenko,[50] D. Derkach,[82] O. Deschamps,[9] F. Dettori,[27,f] B. Dey,[77] A. Di Cicco,[23] P. Di Nezza,[23] S. Didenko,[83] L. Dieste Maronas,[46] H. Dijkstra,[48] V. Dobishuk,[52] C. Dong,[3] A.M. Donohoe,[18] F. Dordei,[27] A.C. dos Reis,[1] L. Douglas,[59] A. Dovbnya,[51] A.G. Downes,[8] M.W. Dudek,[35] L. Dufour,[48] V. Duk,[78] P. Durante,[48] J.M. Durham,[67] D. Dutta,[62] A. Dziurda,[35] A. Dzyuba,[38] S. Easo,[57] U. Egede,[69] V. Egorychev,[41] S. Eidelman,[43,v,†] S. Eisenhardt,[58] S. Ek-In,[49] L. Eklund,[86] S. Ely,[68] A. Ene,[37] E. Epple,[67] S. Escher,[14] J. Eschle,[50] S. Esen,[50] T. Evans,[62] L.N. Falcao,[1] Y. Fan,[6]

JHEP05(2022)067

B. Fang,[73] S. Farry,[60] D. Fazzini,[26,k] M. Féo,[48] A. Fernandez Prieto,[46] A.D. Fernez,[66] F. Ferrari,[20,e] L. Ferreira Lopes,[49] F. Ferreira Rodrigues,[2] S. Ferreres Sole,[32] M. Ferrillo,[50] M. Ferro-Luzzi,[48] S. Filippov,[39] R.A. Fini,[19] M. Fiorini,[21,g] M. Firlej,[34] K.M. Fischer,[63] D.S. Fitzgerald,[87] C. Fitzpatrick,[62] T. Fiutowski,[34] A. Fkiaras,[48] F. Fleuret,[12] M. Fontana,[13] F. Fontanelli,[24,i] R. Forty,[48] D. Foulds-Holt,[55] V. Franco Lima,[60] M. Franco Sevilla,[66] M. Frank,[48] E. Franzoso,[21] G. Frau,[17] C. Frei,[48] D.A. Friday,[59] J. Fu,[6] Q. Fuehring,[15] E. Gabriel,[32] G. Galati,[19,d] A. Gallas Torreira,[46] D. Galli,[20,e] S. Gambetta,[58,48] Y. Gan,[3] M. Gandelman,[2] P. Gandini,[25] Y. Gao,[5] M. Garau,[27] L.M. Garcia Martin,[56] P. Garcia Moreno,[45] J. García Pardiñas,[26,k] B. Garcia Plana,[46] F.A. Garcia Rosales,[12] L. Garrido,[45] C. Gaspar,[48] R.E. Geertsema,[32] D. Gerick,[17] L.L. Gerken,[15] E. Gersabeck,[62] M. Gersabeck,[62] T. Gershon,[56] D. Gerstel,[10] L. Giambastiani,[28] V. Gibson,[55] H.K. Giemza,[36] A.L. Gilman,[63] M. Giovannetti,[23,q] A. Gioventù,[46] P. Gironella Gironell,[45] C. Giugliano,[21,g] K. Gizdov,[58] E.L. Gkougkousis,[48] V.V. Gligorov,[13,48] C. Göbel,[70] E. Golobardes,[85] D. Golubkov,[41] A. Golutvin,[61,83] A. Gomes,[1,a] S. Gomez Fernandez,[45] F. Goncalves Abrantes,[63] M. Goncerz,[35] G. Gong,[3] P. Gorbounov,[41] I.V. Gorelov,[40] C. Gotti,[26] J.P. Grabowski,[17] T. Grammatico,[13] L.A. Granado Cardoso,[48] E. Graugés,[45] E. Graverini,[49] G. Graziani,[22] A. Grecu,[37] L.M. Greeven,[32] N.A. Grieser,[4] L. Grillo,[62] S. Gromov,[83] B.R. Gruberg Cazon,[63] C. Gu,[3] M. Guarise,[21] M. Guittiere,[11] P. A. Günther,[17] E. Gushchin,[39] A. Guth,[14] Y. Guz,[44] T. Gys,[48] T. Hadavizadeh,[69] G. Haefeli,[49] C. Haen,[48] J. Haimberger,[48] S.C. Haines,[55] T. Halewood-leagas,[60] P.M. Hamilton,[66] J.P. Hammerich,[60] Q. Han,[7] X. Han,[17] E.B. Hansen,[62] S. Hansmann-Menzemer,[17] N. Harnew,[63] T. Harrison,[60] C. Hasse,[48] M. Hatch,[48] J. He,[6,b] M. Hecker,[61] K. Heijhoff,[32] K. Heinicke,[15] R.D.L. Henderson,[69,56] A.M. Hennequin,[48] K. Hennessy,[60] L. Henry,[48] J. Heuel,[14] A. Hicheur,[2] D. Hill,[49] M. Hilton,[62] S.E. Hollitt,[15] R. Hou,[7] Y. Hou,[8] J. Hu,[17] J. Hu,[72] W. Hu,[7] X. Hu,[3] W. Huang,[6] X. Huang,[73] W. Hulsbergen,[32] R.J. Hunter,[56] M. Hushchyn,[82] D. Hutchcroft,[60] D. Hynds,[32] P. Ibis,[15] M. Idzik,[34] D. Ilin,[38] P. Ilten,[65] A. Inglessi,[38] A. Ishteev,[83] K. Ivshin,[38] R. Jacobsson,[48] H. Jage,[14] S. Jakobsen,[48] E. Jans,[32] B.K. Jashal,[47] A. Jawahery,[66] V. Jevtic,[15] X. Jiang,[4] M. John,[63] D. Johnson,[64] C.R. Jones,[55] T.P. Jones,[56] B. Jost,[48] N. Jurik,[48] S. Kandybei,[51] Y. Kang,[3] M. Karacson,[48] D. Karpenkov,[83] M. Karpov,[82] J.W. Kautz,[65] F. Keizer,[48] D.M. Keller,[68] M. Kenzie,[56] T. Ketel,[33] B. Khanji,[15] A. Kharisova,[84] S. Kholodenko,[44] T. Kirn,[14] V.S. Kirsebom,[49] O. Kitouni,[64] S. Klaver,[33] N. Kleijne,[29] K. Klimaszewski,[36] M.R. Kmiec,[36] S. Koliiev,[52] A. Kondybayeva,[83] A. Konoplyannikov,[41] P. Kopciewicz,[34] R. Kopecna,[17] P. Koppenburg,[32] M. Korolev,[40] I. Kostiuk,[32,52] O. Kot,[52] S. Kotriakhova,[21,38] P. Kravchenko,[38] L. Kravchuk,[39] R.D. Krawczyk,[48] M. Kreps,[56] S. Kretzschmar,[14] P. Krokovny,[43,v] W. Krupa,[34] W. Krzemien,[36] J. Kubat,[17] M. Kucharczyk,[35] V. Kudryavtsev,[43,v] H.S. Kuindersma,[32,33] G.J. Kunde,[67] T. Kvaratskheliya,[41] D. Lacarrere,[48] G. Lafferty,[62] A. Lai,[27] A. Lampis,[27] D. Lancierini,[50] J.J. Lane,[62] R. Lane,[54] G. Lanfranchi,[23] C. Langenbruch,[14] J. Langer,[15] O. Lantwin,[83] T. Latham,[56] F. Lazzari,[29,r] R. Le Gac,[10] S.H. Lee,[87] R. Lefèvre,[9] A. Leflat,[40] S. Legotin,[83] O. Leroy,[10] T. Lesiak,[35] B. Leverington,[17] H. Li,[72] P. Li,[17] S. Li,[7] Y. Li,[4] Y. Li,[4] Z. Li,[68] X. Liang,[68] T. Lin,[61] R. Lindner,[48] V. Lisovskyi,[15] R. Litvinov,[27] G. Liu,[72] H. Liu,[6] Q. Liu,[6] S. Liu,[4] A. Lobo Salvia,[45] A. Loi,[27] J. Lomba Castro,[46] I. Longstaff,[59] J.H. Lopes,[2] S. López Soliño,[46] G.H. Lovell,[55] Y. Lu,[4] C. Lucarelli,[22,h] D. Lucchesi,[28,m] S. Luchuk,[39] M. Lucio Martinez,[32] V. Lukashenko,[32,52] Y. Luo,[3] A. Lupato,[62] E. Luppi,[21,g] O. Lupton,[56] A. Lusiani,[29,n] X. Lyu,[6] L. Ma,[4] R. Ma,[6] S. Maccolini,[20,e] F. Machefert,[11] F. Maciuc,[37] V. Macko,[49] P. Mackowiak,[15] S. Maddrell-Mander,[54] L.R. Madhan Mohan,[54] O. Maev,[38] A. Maevskiy,[82] M.W. Majewski,[34] J.J. Malczewski,[35] S. Malde,[63] B. Malecki,[35] A. Malinin,[81] T. Maltsev,[43,v] H. Malygina,[17] G. Manca,[27,f] G. Mancinelli,[10] D. Manuzzi,[20,e]

JHEP05(2022)067

D. Marangotto,[25,j] J. Maratas,[9,t] J.F. Marchand,[8] U. Marconi,[20] S. Mariani,[22,h] C. Marin Benito,[48] M. Marinangeli,[49] J. Marks,[17] A.M. Marshall,[54] P.J. Marshall,[60] G. Martelli,[78] G. Martellotti,[30] L. Martinazzoli,[48,k] M. Martinelli,[26,k] D. Martinez Santos,[46] F. Martinez Vidal,[47] A. Massafferri,[1] M. Materok,[14] R. Matev,[48] A. Mathad,[50] V. Matiunin,[41] C. Matteuzzi,[26] K.R. Mattioli,[87] A. Mauri,[32] E. Maurice,[12] J. Mauricio,[45] M. Mazurek,[48] M. McCann,[61] L. Mcconnell,[18] T.H. Mcgrath,[62] N.T. Mchugh,[59] A. McNab,[62] R. McNulty,[18] J.V. Mead,[60] B. Meadows,[65] G. Meier,[15] D. Melnychuk,[36] S. Meloni,[26,k] M. Merk,[32,80] A. Merli,[25,j] L. Meyer Garcia,[2] M. Mikhasenko,[75,c] D.A. Milanes,[74] E. Millard,[56] M. Milovanovic,[48] M.-N. Minard,[8] A. Minotti,[26,k] S.E. Mitchell,[58] B. Mitreska,[62] D.S. Mitzel,[15] A. Mödden ,[15] R.A. Mohammed,[63] R.D. Moise,[61] S. Mokhnenko,[82] T. Mombächer,[46] I.A. Monroy,[74] S. Monteil,[9] M. Morandin,[28] G. Morello,[23] M.J. Morello,[29,n] J. Moron,[34] A.B. Morris,[75] A.G. Morris,[56] R. Mountain,[68] H. Mu,[3] F. Muheim,[58,48] M. Mulder,[79] D. Müller,[48] K. Müller,[50] C.H. Murphy,[63] D. Murray,[62] R. Murta,[61] P. Muzzetto,[27] P. Naik,[54] T. Nakada,[49] R. Nandakumar,[57] T. Nanut,[48] I. Nasteva,[2] M. Needham,[58] N. Neri,[25,j] S. Neubert,[75] N. Neufeld,[48] R. Newcombe,[61] E.M. Niel,[49] S. Nieswand,[14] N. Nikitin,[40] N.S. Nolte,[64] C. Normand,[8] C. Nunez,[87] A. Oblakowska-Mucha,[34] V. Obraztsov,[44] T. Oeser,[14] D.P. O'Hanlon,[54] S. Okamura,[21] R. Oldeman,[27,f] F. Oliva,[58] M.E. Olivares,[68] C.J.G. Onderwater,[79] R.H. O'Neil,[58] J.M. Otalora Goicochea,[2] T. Ovsiannikova,[41] P. Owen,[50] A. Oyanguren,[47] O. Ozcelik,[58] K.O. Padeken,[75] B. Pagare,[56] P.R. Pais,[48] T. Pajero,[63] A. Palano,[19] M. Palutan,[23] Y. Pan,[62] G. Panshin,[84] A. Papanestis,[57] M. Pappagallo,[19,d] L.L. Pappalardo,[21,g] C. Pappenheimer,[65] W. Parker,[66] C. Parkes,[62] B. Passalacqua,[21] G. Passaleva,[22] A. Pastore,[19] M. Patel,[61] C. Patrignani,[20,e] C.J. Pawley,[80] A. Pearce,[48,57] A. Pellegrino,[32] M. Pepe Altarelli,[48] S. Perazzini,[20] D. Pereima,[41] A. Pereiro Castro,[46] P. Perret,[9] M. Petric,[59,48] K. Petridis,[54] A. Petrolini,[24,i] A. Petrov,[81] S. Petrucci,[58] M. Petruzzo,[25] T.T.H. Pham,[68] A. Philippov,[42] R. Piandani,[6] L. Pica,[29,n] M. Piccini,[78] B. Pietrzyk,[8] G. Pietrzyk,[49] M. Pili,[63] D. Pinci,[30] F. Pisani,[48] M. Pizzichemi,[26,k,48] Resmi P.K,[10] V. Placinta,[37] J. Plews,[53] M. Plo Casasus,[46] F. Polci,[13,48] M. Poli Lener,[23] M. Poliakova,[68] A. Poluektov,[10] N. Polukhina,[83,u] I. Polyakov,[68] E. Polycarpo,[2] S. Ponce,[48] D. Popov,[6,48] S. Popov,[42] S. Poslavskii,[44] K. Prasanth,[35] L. Promberger,[48] C. Prouve,[46] V. Pugatch,[52] V. Puill,[11] G. Punzi,[29,o] H. Qi,[3] W. Qian,[6] N. Qin,[3] R. Quagliani,[49] N.V. Raab,[18] R.I. Rabadan Trejo,[6] B. Rachwal,[34] J.H. Rademacker,[54] M. Rama,[29] M. Ramos Pernas,[56] M.S. Rangel,[2] F. Ratnikov,[42,82] G. Raven,[33,48] M. Reboud,[8] F. Redi,[48] F. Reiss,[62] C. Remon Alepuz,[47] Z. Ren,[3] V. Renaudin,[63] R. Ribatti,[29] A.M. Ricci,[27] S. Ricciardi,[57] K. Rinnert,[60] P. Robbe,[11] G. Robertson,[58] A.B. Rodrigues,[49] E. Rodrigues,[60] J.A. Rodriguez Lopez,[74] E.R.R. Rodriguez Rodriguez,[46] A. Rollings,[63] P. Roloff,[48] V. Romanovskiy,[44] M. Romero Lamas,[46] A. Romero Vidal,[46] J.D. Roth,[87] M. Rotondo,[23] M.S. Rudolph,[68] T. Ruf,[48] R.A. Ruiz Fernandez,[46] J. Ruiz Vidal,[47] A. Ryzhikov,[82] J. Ryzka,[34] J.J. Saborido Silva,[46] N. Sagidova,[38] N. Sahoo,[53] B. Saitta,[27,f] M. Salomoni,[48] C. Sanchez Gras,[32] R. Santacesaria,[30] C. Santamarina Rios,[46] M. Santimaria,[23] E. Santovetti,[31,q] D. Saranin,[83] G. Sarpis,[14] M. Sarpis,[75] A. Sarti,[30] C. Satriano,[30,p] A. Satta,[31] M. Saur,[15] D. Savrina,[41,40] H. Sazak,[9] L.G. Scantlebury Smead,[63] A. Scarabotto,[13] S. Schael,[14] S. Scherl,[60] M. Schiller,[59] H. Schindler,[48] M. Schmelling,[16] B. Schmidt,[48] S. Schmitt,[14] O. Schneider,[49] A. Schopper,[48] M. Schubiger,[32] S. Schulte,[49] M.H. Schune,[11] R. Schwemmer,[48] B. Sciascia,[23,48] S. Sellam,[46] A. Semennikov,[41] M. Senghi Soares,[33] A. Sergi,[24,i] N. Serra,[50] L. Sestini,[28] A. Seuthe,[15] Y. Shang,[5] D.M. Shangase,[87] M. Shapkin,[44] I. Shchemerov,[83] L. Shchutska,[49] T. Shears,[60] L. Shekhtman,[43,v] Z. Shen,[5] S. Sheng,[4] V. Shevchenko,[81] E.B. Shields,[26,k] Y. Shimizu,[11] E. Shmanin,[83] J.D. Shupperd,[68] B.G. Siddi,[21] R. Silva Coutinho,[50] G. Simi,[28] S. Simone,[19,d] N. Skidmore,[62] R. Skuza,[17]

JHEP05(2022)067

T. Skwarnicki,[68] M.W. Slater,[53] I. Slazyk,[21,g] J.C. Smallwood,[63] J.G. Smeaton,[55] E. Smith,[50] M. Smith,[61] A. Snoch,[32] L. Soares Lavra,[9] M.D. Sokoloff,[65] F.J.P. Soler,[59] A. Solovev,[38] I. Solovyev,[38] F.L. Souza De Almeida,[2] B. Souza De Paula,[2] B. Spaan,[15] E. Spadaro Norella,[25,j] P. Spradlin,[59] F. Stagni,[48] M. Stahl,[65] S. Stahl,[48] S. Stanislaus,[63] O. Steinkamp,[50,83] O. Stenyakin,[44] H. Stevens,[15] S. Stone,[68,48,†] D. Strekalina,[83] F. Suljik,[63] J. Sun,[27] L. Sun,[73] Y. Sun,[66] P. Svihra,[62] P.N. Swallow,[53] K. Swientek,[34] A. Szabelski,[36] T. Szumlak,[34] M. Szymanski,[48] S. Taneja,[62] A.R. Tanner,[54] M.D. Tat,[63] A. Terentev,[83] F. Teubert,[48] E. Thomas,[48] D.J.D. Thompson,[53] K.A. Thomson,[60] H. Tilquin,[61] V. Tisserand,[9] S. T'Jampens,[8] M. Tobin,[4] L. Tomassetti,[21,g] X. Tong,[5] D. Torres Machado,[1] D.Y. Tou,[3] E. Trifonova,[83] S.M. Trilov,[54] C. Trippl,[49] G. Tuci,[6] A. Tully,[49] N. Tuning,[32,48] A. Ukleja,[36,48] D.J. Unverzagt,[17] E. Ursov,[83] A. Usachov,[32] A. Ustyuzhanin,[42,82] U. Uwer,[17] A. Vagner,[84] V. Vagnoni,[20] A. Valassi,[48] G. Valenti,[20] N. Valls Canudas,[85] M. van Beuzekom,[32] M. Van Dijk,[49] H. Van Hecke,[67] E. van Herwijnen,[83] M. van Veghel,[79] R. Vazquez Gomez,[45] P. Vazquez Regueiro,[46] C. Vázquez Sierra,[48] S. Vecchi,[21] J.J. Velthuis,[54] M. Veltri,[22,s] A. Venkateswaran,[68] M. Veronesi,[32] M. Vesterinen,[56] D. Vieira,[65] M. Vieites Diaz,[49] H. Viemann,[76] X. Vilasis-Cardona,[85] E. Vilella Figueras,[60] A. Villa,[20] P. Vincent,[13] F.C. Volle,[11] D. Vom Bruch,[10] A. Vorobyev,[38] V. Vorobyev,[43,v] N. Voropaev,[38] K. Vos,[80] R. Waldi,[17] J. Walsh,[29] C. Wang,[17] J. Wang,[5] J. Wang,[4] J. Wang,[3] J. Wang,[73] M. Wang,[3] R. Wang,[54] Y. Wang,[7] Z. Wang,[50] Z. Wang,[3] Z. Wang,[6] J.A. Ward,[56,69] N.K. Watson,[53] D. Websdale,[61] C. Weisser,[64] B.D.C. Westhenry,[54] D.J. White,[62] M. Whitehead,[54] A.R. Wiederhold,[56] D. Wiedner,[15] G. Wilkinson,[63] M. K. Wilkinson,[68] I. Williams,[55] M. Williams,[64] M.R.J. Williams,[58] F.F. Wilson,[57] W. Wislicki,[36] M. Witek,[35] L. Witola,[17] G. Wormser,[11] S.A. Wotton,[55] H. Wu,[68] K. Wyllie,[48] Z. Xiang,[6] D. Xiao,[7] Y. Xie,[7] A. Xu,[5] J. Xu,[6] L. Xu,[3] M. Xu,[56] Q. Xu,[6] Z. Xu,[9] Z. Xu,[6] D. Yang,[3] S. Yang,[6] Y. Yang,[6] Z. Yang,[5] Z. Yang,[66] Y. Yao,[68] L.E. Yeomans,[60] H. Yin,[7] J. Yu,[71] X. Yuan,[68] O. Yushchenko,[44] E. Zaffaroni,[49] M. Zavertyaev,[16,u] M. Zdybal,[35] O. Zenaiev,[48] M. Zeng,[3] D. Zhang,[7] L. Zhang,[3] S. Zhang,[71] S. Zhang,[5] Y. Zhang,[5] Y. Zhang,[63] A. Zharkova,[83] A. Zhelezov,[17] Y. Zheng,[6] T. Zhou,[5] X. Zhou,[6] Y. Zhou,[6] V. Zhovkovska,[11] X. Zhu,[3] X. Zhu,[7] Z. Zhu,[6] V. Zhukov,[14,40] Q. Zou,[4] S. Zucchelli,[20,e] D. Zuliani,[28] G. Zunica[62]

[1] *Centro Brasileiro de Pesquisas Físicas (CBPF), Rio de Janeiro, Brazil*
[2] *Universidade Federal do Rio de Janeiro (UFRJ), Rio de Janeiro, Brazil*
[3] *Center for High Energy Physics, Tsinghua University, Beijing, China*
[4] *Institute Of High Energy Physics (IHEP), Beijing, China*
[5] *School of Physics State Key Laboratory of Nuclear Physics and Technology, Peking University, Beijing, China*
[6] *University of Chinese Academy of Sciences, Beijing, China*
[7] *Institute of Particle Physics, Central China Normal University, Wuhan, Hubei, China*
[8] *Univ. Savoie Mont Blanc, CNRS, IN2P3-LAPP, Annecy, France*
[9] *Université Clermont Auvergne, CNRS/IN2P3, LPC, Clermont-Ferrand, France*
[10] *Aix Marseille Univ, CNRS/IN2P3, CPPM, Marseille, France*
[11] *Université Paris-Saclay, CNRS/IN2P3, IJCLab, Orsay, France*
[12] *Laboratoire Leprince-Ringuet, CNRS/IN2P3, Ecole Polytechnique, Institut Polytechnique de Paris, Palaiseau, France*
[13] *LPNHE, Sorbonne Université, Paris Diderot Sorbonne Paris Cité, CNRS/IN2P3, Paris, France*
[14] *I. Physikalisches Institut, RWTH Aachen University, Aachen, Germany*
[15] *Fakultät Physik, Technische Universität Dortmund, Dortmund, Germany*
[16] *Max-Planck-Institut für Kernphysik (MPIK), Heidelberg, Germany*
[17] *Physikalisches Institut, Ruprecht-Karls-Universität Heidelberg, Heidelberg, Germany*
[18] *School of Physics, University College Dublin, Dublin, Ireland*

JHEP05(2022)067

[19] *INFN Sezione di Bari, Bari, Italy*
[20] *INFN Sezione di Bologna, Bologna, Italy*
[21] *INFN Sezione di Ferrara, Ferrara, Italy*
[22] *INFN Sezione di Firenze, Firenze, Italy*
[23] *INFN Laboratori Nazionali di Frascati, Frascati, Italy*
[24] *INFN Sezione di Genova, Genova, Italy*
[25] *INFN Sezione di Milano, Milano, Italy*
[26] *INFN Sezione di Milano-Bicocca, Milano, Italy*
[27] *INFN Sezione di Cagliari, Monserrato, Italy*
[28] *Universita degli Studi di Padova, Universita e INFN, Padova, Padova, Italy*
[29] *INFN Sezione di Pisa, Pisa, Italy*
[30] *INFN Sezione di Roma La Sapienza, Roma, Italy*
[31] *INFN Sezione di Roma Tor Vergata, Roma, Italy*
[32] *Nikhef National Institute for Subatomic Physics, Amsterdam, Netherlands*
[33] *Nikhef National Institute for Subatomic Physics and VU University Amsterdam, Amsterdam, Netherlands*
[34] *AGH - University of Science and Technology, Faculty of Physics and Applied Computer Science, Kraków, Poland*
[35] *Henryk Niewodniczanski Institute of Nuclear Physics Polish Academy of Sciences, Kraków, Poland*
[36] *National Center for Nuclear Research (NCBJ), Warsaw, Poland*
[37] *Horia Hulubei National Institute of Physics and Nuclear Engineering, Bucharest-Magurele, Romania*
[38] *Petersburg Nuclear Physics Institute NRC Kurchatov Institute (PNPI NRC KI), Gatchina, Russia*
[39] *Institute for Nuclear Research of the Russian Academy of Sciences (INR RAS), Moscow, Russia*
[40] *Institute of Nuclear Physics, Moscow State University (SINP MSU), Moscow, Russia*
[41] *Institute of Theoretical and Experimental Physics NRC Kurchatov Institute (ITEP NRC KI), Moscow, Russia*
[42] *Yandex School of Data Analysis, Moscow, Russia*
[43] *Budker Institute of Nuclear Physics (SB RAS), Novosibirsk, Russia*
[44] *Institute for High Energy Physics NRC Kurchatov Institute (IHEP NRC KI), Protvino, Russia, Protvino, Russia*
[45] *ICCUB, Universitat de Barcelona, Barcelona, Spain*
[46] *Instituto Galego de Física de Altas Enerxías (IGFAE), Universidade de Santiago de Compostela, Santiago de Compostela, Spain*
[47] *Instituto de Fisica Corpuscular, Centro Mixto Universidad de Valencia - CSIC, Valencia, Spain*
[48] *European Organization for Nuclear Research (CERN), Geneva, Switzerland*
[49] *Institute of Physics, Ecole Polytechnique Fédérale de Lausanne (EPFL), Lausanne, Switzerland*
[50] *Physik-Institut, Universität Zürich, Zürich, Switzerland*
[51] *NSC Kharkiv Institute of Physics and Technology (NSC KIPT), Kharkiv, Ukraine*
[52] *Institute for Nuclear Research of the National Academy of Sciences (KINR), Kyiv, Ukraine*
[53] *University of Birmingham, Birmingham, United Kingdom*
[54] *H.H. Wills Physics Laboratory, University of Bristol, Bristol, United Kingdom*
[55] *Cavendish Laboratory, University of Cambridge, Cambridge, United Kingdom*
[56] *Department of Physics, University of Warwick, Coventry, United Kingdom*
[57] *STFC Rutherford Appleton Laboratory, Didcot, United Kingdom*
[58] *School of Physics and Astronomy, University of Edinburgh, Edinburgh, United Kingdom*
[59] *School of Physics and Astronomy, University of Glasgow, Glasgow, United Kingdom*
[60] *Oliver Lodge Laboratory, University of Liverpool, Liverpool, United Kingdom*
[61] *Imperial College London, London, United Kingdom*
[62] *Department of Physics and Astronomy, University of Manchester, Manchester, United Kingdom*
[63] *Department of Physics, University of Oxford, Oxford, United Kingdom*
[64] *Massachusetts Institute of Technology, Cambridge, MA, United States*

JHEP05(2022)067

[65] University of Cincinnati, Cincinnati, OH, United States
[66] University of Maryland, College Park, MD, United States
[67] Los Alamos National Laboratory (LANL), Los Alamos, United States
[68] Syracuse University, Syracuse, NY, United States
[69] School of Physics and Astronomy, Monash University, Melbourne, Australia, associated to [56]
[70] Pontifícia Universidade Católica do Rio de Janeiro (PUC-Rio), Rio de Janeiro, Brazil, associated to [2]
[71] Physics and Micro Electronic College, Hunan University, Changsha City, China, associated to [7]
[72] Guangdong Provincial Key Laboratory of Nuclear Science, Guangdong-Hong Kong Joint Laboratory of Quantum Matter, Institute of Quantum Matter, South China Normal University, Guangzhou, China, associated to [3]
[73] School of Physics and Technology, Wuhan University, Wuhan, China, associated to [3]
[74] Departamento de Fisica, Universidad Nacional de Colombia, Bogota, Colombia, associated to [13]
[75] Universität Bonn - Helmholtz-Institut für Strahlen und Kernphysik, Bonn, Germany, associated to [17]
[76] Institut für Physik, Universität Rostock, Rostock, Germany, associated to [17]
[77] Eotvos Lorand University, Budapest, Hungary, associated to [48]
[78] INFN Sezione di Perugia, Perugia, Italy, associated to [21]
[79] Van Swinderen Institute, University of Groningen, Groningen, Netherlands, associated to [32]
[80] Universiteit Maastricht, Maastricht, Netherlands, associated to [32]
[81] National Research Centre Kurchatov Institute, Moscow, Russia, associated to [41]
[82] National Research University Higher School of Economics, Moscow, Russia, associated to [42]
[83] National University of Science and Technology "MISIS", Moscow, Russia, associated to [41]
[84] National Research Tomsk Polytechnic University, Tomsk, Russia, associated to [41]
[85] DS4DS, La Salle, Universitat Ramon Llull, Barcelona, Spain, associated to [45]
[86] Department of Physics and Astronomy, Uppsala University, Uppsala, Sweden, associated to [59]
[87] University of Michigan, Ann Arbor, United States, associated to [68]

[a] Universidade Federal do Triângulo Mineiro (UFTM), Uberaba-MG, Brazil
[b] Hangzhou Institute for Advanced Study, UCAS, Hangzhou, China
[c] Excellence Cluster ORIGINS, Munich, Germany
[d] Università di Bari, Bari, Italy
[e] Università di Bologna, Bologna, Italy
[f] Università di Cagliari, Cagliari, Italy
[g] Università di Ferrara, Ferrara, Italy
[h] Università di Firenze, Firenze, Italy
[i] Università di Genova, Genova, Italy
[j] Università degli Studi di Milano, Milano, Italy
[k] Università di Milano Bicocca, Milano, Italy
[l] Università di Modena e Reggio Emilia, Modena, Italy
[m] Università di Padova, Padova, Italy
[n] Scuola Normale Superiore, Pisa, Italy
[o] Università di Pisa, Pisa, Italy
[p] Università della Basilicata, Potenza, Italy
[q] Università di Roma Tor Vergata, Roma, Italy
[r] Università di Siena, Siena, Italy
[s] Università di Urbino, Urbino, Italy
[t] MSU - Iligan Institute of Technology (MSU-IIT), Iligan, Philippines
[u] P.N. Lebedev Physical Institute, Russian Academy of Science (LPI RAS), Moscow, Russia
[v] Novosibirsk State University, Novosibirsk, Russia
[†] Deceased

JHEP05(2022)067